Journal of Molecular Catalysis A: Chemical 398 (2015) 50–57

Contents lists available at ScienceDirect

Journal of Molecular Catalysis A: Chemical

journal homepage: www.elsevier.com/locate/molcata

Self-condensation of acetone over Mg–Al layered double hydroxide supported on multi-walled carbon nanotube catalysts

Almudena Celaya-Sanfiz[a,b], Nicolás Morales-Vega[c], Martina De Marco[a], Diana Iruretagoyena[c], Mohamed Mokhtar[d], Salem M. Bawaked[d], Sulaiman N. Basahel[d], Shaeel A. Al-Thabaiti[d], Abdulrahman O. Alyoubi[d], Milo S.P. Shaffer[a,*]

[a] Department of Chemistry, Imperial College London, South Kensington Campus, London SW7 2AZ, UK
[b] Bio Nano Consulting, The Gridiron Building, One Pancras Square, London, N1C 4AG
[c] Department of Chemical Engineering, Imperial College London, South Kensington Campus, London SW7 2AZ, UK
[d] Department of Chemistry, Faculty of Science, King Abdulaziz University, Saudi Arabia

ARTICLE INFO

Article history:
Received 25 June 2014
Received in revised form 2 October 2014
Accepted 3 November 2014
Available online 20 November 2014

Keywords:
Self condensation
Catalysis
Carbon nanotubes
Layered double hydroxide

ABSTRACT

Mg–Al (2:1) layered double hydroxides (LDH) were supported onto multi-walled carbon nanotubes (MWNTs), in order to optimize the catalytic performance of these solid base catalysts. The resulting LDH/MWNT hybrids after activation (heat-treatment/hydration) were compared to the pure activated LDH catalyst for the self-condensation of acetone. Smaller LDH crystallite sizes and a good dispersion of the LDH particles on the MWNTs increase the number of active centers accessible to acetone, and hence enhance activity. However, debris created during MWNT oxidation inhibits the reaction, leading to an optimum intermediate hybrid composition.

© 2014 Elsevier B.V. All rights reserved.

1. Introduction

Base-catalyzed aldol condensation is a common method for coupling organic molecules via C—C bond formation. The aldol addition of acetone to produce diacetone alcohol (DAA) is a typical reaction, which is both a model and important in its own right. DAA is widely used as a solvent in both consumer and industrial products, for example in hydraulic fluids and styrene-butadiene latex paints [1]. DAA is industrially produced by a homogeneous process using soda or potash as the base catalyst [2]. However, homogeneous catalysts can be difficult to separate after reaction and therefore these processes are not considered to be environmentally friendly [3]. Conversely, heterogeneous catalysts can be separated from products easily and reused, thus making processes "greener" since the waste stream is reduced. Therefore, the application of such catalysts has attracted much attention in the fine chemicals industry [3–5]. Amongst the solid base catalysts investigated for the catalysis of the self-condensation of acetone for the production of DAA, layered double hydroxides (LDHs), specifically Mg–Al-LDH, are reported to be promising candidates [5–11].

LDHs, also known as hydrotalcite-like compounds, are a class of synthetic anionic clays whose structure is based on brucite ($Mg(OH)_2$)-like layers [12], where some divalent cations are replaced by trivalent ions, giving positively-charged sheets. This charge is balanced by the intercalation of anions (e.g. CO_3^{2-}) in the hydrated interlayer regions. Their general formula is $[M(II)_{1-x}M(III)_x(OH)_2]^{x+}[A_{x/m}{}^{m-}]\cdot nH_2O$ where the ratio between the di- and trivalent cations can range between $1.5 < M(II)/M(III) < 4$. Typical cations include Mg^{2+}, Zn^{2+}, Cu^{2+} and Ni^{2+}, and Al^{3+}, Fe^{3+}, Cr^{3+} and Ga^{3+} on the M(II) and M(III) sites, respectively. The catalytic properties of Mg–Al-LDHs are influenced by their physical and chemical characteristics, particularly their high surface area, temperature stability, and distribution of acid-basic strengths [12]. These properties are determined primarily during synthesis and subsequent specific activation reactions. Activation of Mg–Al-LDH via heat treatment has been widely studied and the resulting Mg–Al mixed metal oxides have been extensively investigated for a variety of reactions [5,7,10,13–17]. Meixnerite-like forms of LDH, where the calcined LDH is hydrated in an inert atmosphere to introduce OH^- instead of CO_3^{2-}, have been shown to be most active [6,8–16,18–22]. In this work, the term "hydration" [23] will be used instead of "rehydration", to make clear that the LDH interlayer counter anion is OH^- (meixnerite-like) rather than the native CO_3^{2-}. Both liquid and gas phase hydration procedures

* Corresponding author. Tel.: +44 (0) 20 7594 5825.
E-mail address: m.shaffer@imperial.ac.uk (M.S.P. Shaffer).

http://dx.doi.org/10.1016/j.molcata.2014.11.002
1381-1169/© 2014 Elsevier B.V. All rights reserved.

have been investigated previously, with the former being shown to generate a more active catalyst for liquid phase condensation reactions [6,20,24,25]. This increased activity is attributed to the OH^- Brønsted basic sites which are involved in the catalysis and found on the edges of the platelets; thus by generating smaller LDH crystallite sizes, the activity of the catalyst is enhanced [20]. Attempts have been made to increase the activity further, either by increasing the number of active sites through varying synthesis processes to alter platelet sizes [18,26], or by increasing the particle dispersion, thus improving the accessibility of the active sites [24,25,27,28]. Winter et al. [24,25], and more recently Alvarez et al. [28], have demonstrated that Mg–Al-LDHs supported on carbon nanofibres (CNFs) have an improved catalytic activity for the self-condensation of acetone. Given these promising results, it is of interest to use well-understood, commercially-available carbon nanomaterials, rather than in house academic research products; by exploring the effect of carbon to LDH ratio, any optimum composition can be identified.

Multi-walled carbon nanotubes (MWNTs) are an example of a commercially-available carbon nanomaterial that can be purchased from a number of companies in relatively large quantities. MWNTs have been used as a catalyst supports previously [29] and offer some advantages over CNFs. The morphology of (commercial) MWNTs tends to be more defined, with a smaller diameter (typically ~10 nm) than CNFs, and hence higher surface area. MWNTs also have an enhanced robustness as the graphitic layers mainly lie parallel to the tube axis, whereas the CNFs can easily fracture along the oblique basal planes due to the intrinsically 'herringbone' structure. The aspect ratio (i.e. length/diameter ratio) of MWNTs is high and remains so during subsequent usage. Thus, the effective open framework of the MWNTs is retained, which in turn should improve both catalyst dispersion and reagent accessibility. The mesoporosity of MWNT networks is likely to facilitate mass transport, and their significant electrical conductivity could offer new opportunities for monitoring and catalyst regeneration.

In this study, LDH materials were supported on typical, commercially-available, CVD-grown MWNTs, following functionalization, in order to optimize the catalytic performance of these solid base catalysts. Acid oxidation has been previously found to assist the deposition of LDHs on both CNFs and MWNTs [24,25,30], by providing a polar, charged surface compatible with the hydroxides. Four hybrid materials were prepared by systematically increasing the MWNT-content, for the purpose of identifying underlying trends relevant to catalytic applications. The resulting MWNT/LDH hybrids after activation (heat-treatment/hydration) were compared to the pure LDH catalyst for the self-condensation of acetone. The influence of the support on the bulk and surface properties of the LDH materials and subsequent catalytic behavior was investigated.

2. Experimental

2.1. Catalyst preparation

LDHs were synthesized via precipitation, as previously reported [30]. An aqueous solution (50 mL) of 0.1 mol $Mg(NO_3)_2{\cdot}6H_2O$ (Sigma–Aldrich) and 0.05 mol $Al(NO_3)_3{\cdot}9H_2O$ (Sigma–Aldrich) was added to an aqueous solution (75 mL) containing 0.35 mol of NaOH (AnalaR) and 0.09 mol of Na_2CO_3 (Riedel-de Haen). The resultant white suspension was then heated to 333 K and stirred at 300 rpm for 12 h. The precipitate obtained was filtered using 0.4 μm polycarbonate membranes (Millipore, HTTP Isopore membrane) and washed with 500 mL of water at 333 K. The white precipitate was then dried for 12 h at 393 K. Mg–Al-LDH (i.e. 100wt% LDH) was prepared to act as reference material. A 2:1 ratio of Mg:Al was used in all cases as it is reported to be more active for the self-condensation of acetone than the conventional 3:1 ratio [29].

In order to support the LDHs on MWNTs (ARKEMA Graphistrength® product), the MWNTs were first oxidized. 7 mL of a 3:1 mixture of concentrated H_2SO_4/HNO_3 was added for each 200 mg MWNTs; the ratio of carbon to acid has previously been found to determine the nature of the product and was thus kept constant [31]. The mixture was stirred and refluxed for 30 min. After cooling, the nanotubes were recovered from the supernatant by filtration using 0.4 μm polycarbonate membranes and washed with 500 mL of 0.01 M NaOH [32]. The solution was then washed with distilled water until the filtrate reached a neutral pH. The oxidized MWNTs were then dispersed in an aqueous solution (2.06 mL) containing 9.9 mmol NaOH and 2.5 mmol Na_2CO_3. This solution was then titrated with 1.39 mL of a salt solution of 2.8 mmol $Mg(NO_3)_2{\cdot}6H_2O$ and 1.4 mmol $Al(NO_3)_3{\cdot}9H_2O$. The resulting black suspension was aged at 333 K, and stirred at 300 rpm for 12 h. The sample was filtered using 0.4 μm polycarbonate membranes and washed with 500 mL of water at 333 K and then dried for 12 h at 393 K. A pure LDH control, and four different MWNT/LDH hybrids were prepared with theoretical MWNT weight percentages [MWNT:LDH ratio] of 20 wt% [1:4], 33 wt% [1:2], 50 wt% [1:1] and 67 wt% [2:1].

For the carbonaceous debris experiments, the debris were extracted from 300 mg of dilute base washed, oxidized MWNTs by treating them in 2.06 mL 4.8 M NaOH and stirring at 333 K for 12 h, thus reproducing the LDH synthesis conditions. The solubilized debris in base solution was separated from the remaining nanotubes through a 0.4 μm polycarbonate filter, and used as the feedstock in an otherwise standard LDH synthesis procedure. Within the limitations of this procedure, the debris content was approximately equivalent to the MWNT/LDH_{hl}-50 [1:1] sample.

2.2. Catalyst activation

The LDH samples were activated via a two-step process: heat treatment in inert atmosphere followed by hydration. The first step, heat treatment, was always carried out in nitrogen with a flow of 100 mL min^{-1} for 6 h at 723 K (heating rate 10 K min^{-1}). The second was a liquid phase hydration where the heat-treated samples were heated in decarbonated water at 303 K and stirred at 700 rpm for 1 h in an inert atmosphere [6]. Subsequently, the temperature was ramped up to 373 K, and the reaction was held at this temperature for a further 2 h under inert atmosphere, without stirring. The remaining water was filtered off via cannula filtration under nitrogen and finally the resulting solid was dried at 303 K overnight under nitrogen. The activated MWNT/LDH hybrids were labeled as follows: MWNT/LDH_{hl}-20, MWNT/LDH_{hl}-33, MWNT/LDH_{hl}-50 and MWNT/LDH_{hl}-67, depending on the intended weight percentage of MWNTs in each sample.

2.3. Characterization

The phase composition of the catalysts was determined by X-ray diffraction (XRD) performed on a PANalytical X'Pert Pro Multi Purpose Diffractometer using Cu-Kα radiation. Thermogravimetric analysis (TGA) was performed using a Perkin Elmer Pyris apparatus. The samples (3 mg) were initially outgassed at 373 K under N_2 for 20 min and subsequently heated from 373 K to 1073 K in air (20 mL min^{-1}) at 10 K min^{-1}. Morphology studies were performed, using a Gemini 1525 FEG-Scanning Electron Microscope (5 kV, SEI image) fitted with an Oxford Instruments INCA energy dispersive X-ray spectrometer (EDS); for scanning electron microscopy (SEM) investigations, MWNT/LDH_{hl} samples were deposited on silver paint. The microstructure of the catalysts was investigated by transmission electron microscopy (TEM) using a JEOL2010 Transmission

Electron Microscope operating at 200 kV; here, samples were prepared by dispersing the sample in isopropanol using 0.01 mg of MWNT/LDH_{hl} per mL of solvent, and allowing a drop to dry onto a copper grid coated with holey carbon film (300 mesh, Agar Scientific). Nitrogen adsorption measurements were performed at 77 K using a Tristar 3000 Micrometrics instrument, and analyzed with the Tristar 3000 v6.04 software. Specific surface areas were calculated according to the Brunauer, Emmet and Teller (BET) equation from the adsorption isotherm. The pore-size distribution of MWNT/LDH_{hl} samples was calculated from desorption branch using the Barrett–Joyner–Halenda (BJH) method. Temperature-programmed desorption (TPD) experiments on the unsupported LDHs and MWNT/LDH_{hl} composites were performed to estimate the strength of the basic centers and the density and concentration of surface basic sites. An atmospheric pressure microreactor connected to a mass spectrometer via a heated quartz capillary was used for TPD. The catalyst (20 mg) was heated at 393 K (10 K min^{-1}) in flowing argon for 1 h in order to remove the physically adsorbed water. The sample was then cooled to 303 K and exposed to CO_2 (20% CO_2 in argon) for 1 h. After this, the system was purged in flowing argon for 2 h to remove any physisorbed CO_2 and then the temperature was increased, from 303 K to 1273 K at 50 K min^{-1}. The concentration of the CO_2 desorbed into the argon carrier gas was monitored with the mass spectrometer. The amount of CO_2 was quantified by comparing the area under the TPD profile to the peak areas of the CO_2 calibration pulses injected before each TPD experiment.

2.4. Catalysis

The self-condensation of acetone was performed in a double-walled, thermostatically temperature-controlled, glass reactor (volume = 60 mL and diameter = 4 cm) for 100 h. Typically, 0.009 mol of iso-octane, used as internal standard, was added to 0.8 mol of acetone. The resulting mixture was cooled to the reaction temperature, 273 K. Once the temperature was stable, the freshly activated catalyst was introduced into the reactor and then this mixture was mechanically stirred at 900 rpm. The transfer of the catalyst from the hydration setup to the reactor was handled in order to avoid, as much as possible, CO_2 contamination due to air exposure. This procedure was performed identically for each sample. Both cooling and reaction were carried out under nitrogen. The mass of the total catalyst was altered in order to keep the mass of the LDH constant at 50 mg in all cases. Aliquots of 0.5 mL were taken from the reaction mixture and diluted with 0.5 mL of diethyl acetate at regular periods and analyzed offline by a Varian Gas Chromatograph (GC) equipped with a DB-624 capillary column and a flame ionization detector.

3. Results and discussion

3.1. Catalyst characterization

Four different hydrated MWNT/LDH catalysts were prepared with intentionally varied MWNT weight percentages (MWNT/LDH_{hl}-20, MWNT/LDH_{hl}-33, MWNT/LDH_{hl}-50 and MWNT/LDH_{hl}-67). The actual MWNT weight percentage for each sample was obtained via TGA. The TGA decomposition profile for pure LDH_{hl} shows two weight loss events. The first, at 373–473 K, corresponds to the removal of the remaining physically-adsorbed and interlayer water, and the second, in the range 473–773 K, is related to the dehydroxylation of the layered structure and decomposition of the interlayer carbonates (Fig. 1) [6]. In comparison with LDH_{hl}, the MWNT/LDH_{hl} samples show an additional third weight loss at 773–973 K, due to the oxidation

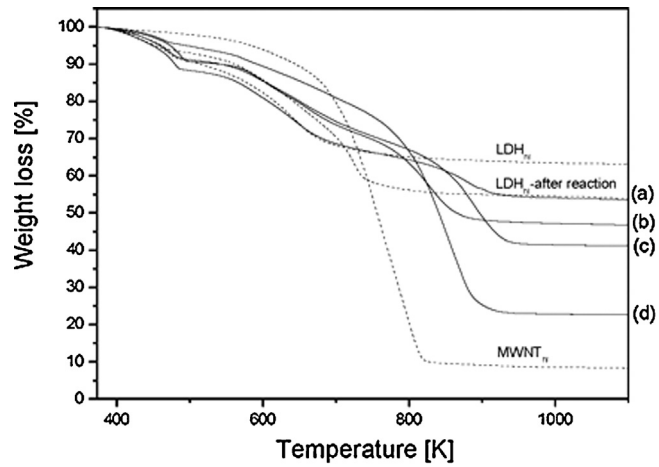

Fig. 1. Thermogravimetic analysis of LDH_{hl}, LDH_{hl}-after reaction, $MWNT_{hl}$ and MWNT/LDH_{hl} samples: (a) MWNT/LDH_{hl}-20, (b) MWNT/LDH_{hl}-33, (c) MWNT/LDH_{hl}-50, and (d) MWNT/LDH_{hl}-67.

of the $MWNT_{hl}$. The TGA residues of pure LDH_{hl} and $MWNT_{hl}$ were used to estimate the actual LDH weight percentage in each catalyst, assuming that the residues from each phase are simply additive (Table 1). The small differences between the measured and intended MWNT weight percentages in the MWNT/LDH_{hl} compositions can be attributed to a partial loss of nanotubes during the filtration step of the synthesis procedure [30]. As expected, the residues of the hydrated MWNT/LDH_{hl} samples increase with increasing weight percentage of MWNT (Fig. 1), as was also observed for the as-synthesized hybrids [30].

Layered double hydroxide (LDH) structures were confirmed by XRD for both the as-synthesized and hydrated LDH samples (LDH as-synthesized and LDH_{hl} respectively in Fig. 2). Both show the typical layered structure features identified in the LDH powder data (JPDS 14–191). The lattice parameters of both samples were determined to be a = 2.98 Å and c = 22.39 Å for the as-synthesized LDH, and a = 2.98 Å and c = 22.48 Å for the hydrated LDH, which differ from the more commonly reported Mg–Al-LDH (3:1 = Mg:Al) samples, as expected, since the lattice parameters depend on the LDH composition [33]. The in-plane lattice parameter, a, is comparable for the as-synthesized and hydrated samples (a = 2.98 Å), however, the out-of-plane lattice parameter, c, for the hydrated LDH

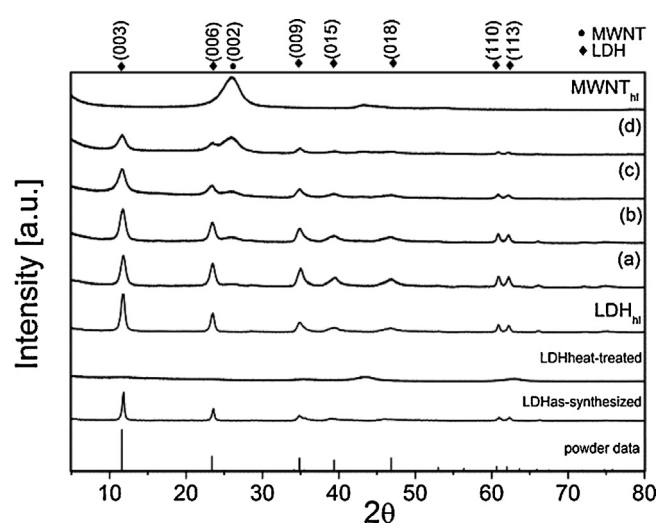

Fig. 2. X-ray diffraction patterns of LDH power data, $LDH_{as\text{-}synthesized}$, $LDH_{heat\text{-}treated}$, LDH_{hl}, MWNT/LDH_{hl} samples: (a) MWNT/LDH_{hl}-20, (b) MWNT/LDH_{hl}-33, (c) MWNT/LDH_{hl}-50, and (d) MWNT/LDH_{hl}-67, and $MWNT_{hl}$.

Table 1
Actual MWNT weight percentage, initial reaction rate and CO_2 adsorption for each catalyst.

Sample	MWNT wt% (theoretical)	Initial rate[a] ($mmol_{DAA}\ g_{LDH}^{-1}\ h^{-1}$)	Initial rate ($mmol_{DAA}\ g_{cat}^{-1}\ h^{-1}$)	$mmol_{CO2}\ g_{LDH}^{-1}$	$mmol_{CO2}\ g_{cat}^{-1}$	$mmol_{acetone}$ $mmol_{total\ desorbed\ CO2}^{-1}\ h^{-1}$
LDH_{hl}	0 (0)	71.1 ± 11	71.1 ± 11	1.4	1.4	71.2
MWNT/LDH_{hl}-20	17 (20)	196.2 ± 20	162.7 ± 20	1.8	1.5	218
MWNT/LDH_{hl}-33	30 (33)	110.0 ± 3	77 ± 3	1.6	1.1	139.2
MWNT/LDH_{hl}-50	40 (50)	123.2 ± 20	73.8 ± 20	2.4	1.4	102.2
MWNT/LDH_{hl}-67	67 (67)	9.8 ± 3	3.2 ± 3	1.9	0.6	10.4
Debris	N/A	8.3 ± 1		N/A	N/A	N/A

[a] The initial rate values are calculated as the amount of DAA produced per hour and per unit mass of LDH with the error estimated by polynomial fitting.

is slightly bigger than that of the as-synthesized LDH (c = 22.48 Å and c = 22.39 Å, respectively). This difference in the c lattice parameter is probably due to the presence of a different counter anion located in the interlayer (OH^- and CO_3^{2-}, respectively). Upon heat-treatment at 723 K in inert gas (LDH heat-treated in Fig. 2), the structure collapses to form a mixed oxide phase ($MgAlO_x$, periclase-like structure, JCPDS 87-0653). Subsequent hydration in liquid phase allows the reformation of the original structure (LDH_{hl} in Fig. 2), although OH^- groups are expected to replace the original carbonates. The interlayer carbonates of the as-synthesized LDH are removed during heat treatment, and upon hydration, OH^- groups may be formed in the interlayer instead, thus creating Brønsted base sites within the reformed layered structure [12]. The presence of MWNTs in the MWNT/LDH_{hl} hybrid catalysts does not change the bulk crystal structure of the LDH (Fig. 2a–d). However, the width of the LDH peaks increases and the position of the (0 0 3) reflection shifts to lower 2θ on increasing MWNT weight percentage. The additional peak at 26.3° 2θ belongs to interlayer graphitic spacing in MWNTs, as can be observed in the diffractogram of pure $MWNT_{hl}$ ($MWNT_{hl}$ in Fig. 2); the intensity of this peak increases relative to the LDH peaks, as expected, on increasing the MWNT content. The shift of the (0 0 3) LDH reflection to lower 2θ (i.e. increased layer spacing), may relate to an increase in disorder, possibly the insertion of carboxylated debris from the oxidized MWNTs (discussed further below) into the CO_3^{2-} interlayer sites during the original synthesis. The crystallite size of the LDH hexagonal-platelets, can be calculated using the Scherrer equation [33] but here may underestimate the physical particle size as a result of polydispersity, significant peak broadening by defects including stacking faults and point defects, or simple bending of the platelets. As such, the lateral and through-thickness dimensions calculated from the (1 1 0) and (0 0 3) reflections, respectively, can be considered as the 'apparent' crystallite size [12]. After activation (Fig. 3), apparent LDH crystallites sizes are either constant or increase in the lateral dimension, whereas in the c direction they are constant or decrease. These contrasting trends suggest that there is a real change in crystallite size, although a variation in the nature or concentration of defects [34] may also play a role. The apparent crystallite size in c direction is in reasonable agreement with the information obtained from electron microscopy (see Electron microscopy section). However, the calculated size in the lateral dimension is smaller than that observed in the images, and likely to be due to the effects mentioned above. Particularly bending pure LDH is smaller in the c direction after activation, but lateral dimensions are unchanged. Upon addition of MWNT, the sizes in both directions are systematically reduced compared to the as-synthesized samples, probably as a result of heterogeneous nucleation effects during the initial synthesis. After activation, the same trends are evident although weaker; in this case, during the recrystallisation process, it appears that the product is more sensitive to the presence MWNTs rather than their exact mass. Ultimately, the hydrated hybrids contain relatively thinner and smaller LDH platelets compared to the pure hydrated LDH (Table 2).

Table 2
Physico-chemical properties of the various MWNT/LDH_{hl} materials, LDH_{hl} and $MWNT_{hl}$ determined by nitrogen physisorption and TGA. Crystallite sizes are shown in Fig. 3.

Sample	S_{BET} ($m^2\ g^{-1}$)[a]	V_{meso} ($cm^3\ g^{-1}$)	HT loading (%)
$MWNT_{hl}$	230	0.68	0
MWNT/LDH_{hl}-20	119	0.38	17 (20)
MWNT/LDH_{hl}-33	127	0.34	30 (33)
MWNT/LDH_{hl}-50	93	0.35	40 (50)
MWNT/LDH_{hl}-67	85	0.62	67 (67)
LDH_{hl}	44	0.27	100

[a] No micropores observed (t-plot).

The pure LDH_{hl} material shows the typical hexagonal-platelet morphology, in agreement with the literature [12], and consistent with the crystallographic information discussed previously. The hexagonal-platelet morphology of the LDH particles is maintained in the hybrid samples. SEM images of the different supported materials (Fig. 4, and Supplementary data) show a uniform distribution of LDH platelets across the MWNTs in all samples, with the exception of the MWNT/LDH_{hl}-67 sample in which some segregation of both phases seems to occur. The LDH particles appear to be nucleated on and grow within the open framework of the MWNTs which acts as a supporting scaffold. Due to the high aspect ratio but differing geometry (1D vs. 2D) of the two components, the area of contact between the particles is relatively small. For this reason, direct catalyst–support interactions may be less significant, but physicochemical aspects, such as enhanced accessibility and reduced sintering, may be particularly improved. Whether the system can be considered a "supported–catalyst" in a traditional sense

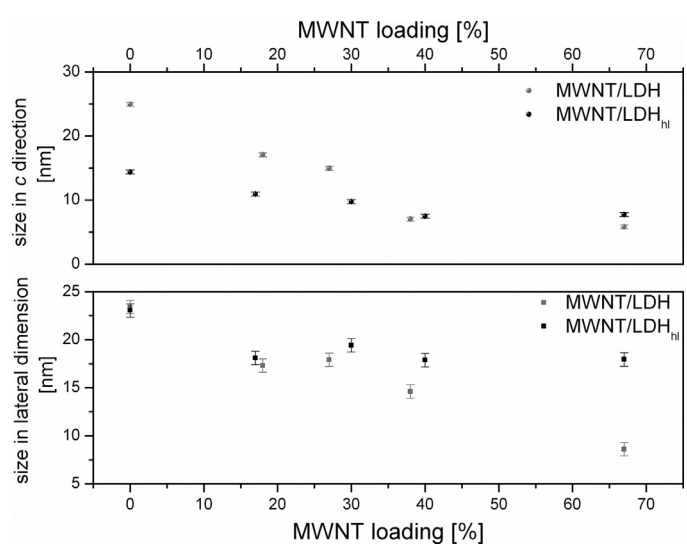

Fig. 3. LDH apparent crystallite size (Scherrer equation) calculated from the (1 1 0) reflection (lateral dimension) and the (0 0 3) reflection (c direction) of MWNT/LDH and MWNT/LDH_{hl} samples vs. MWNT loading (wt%).

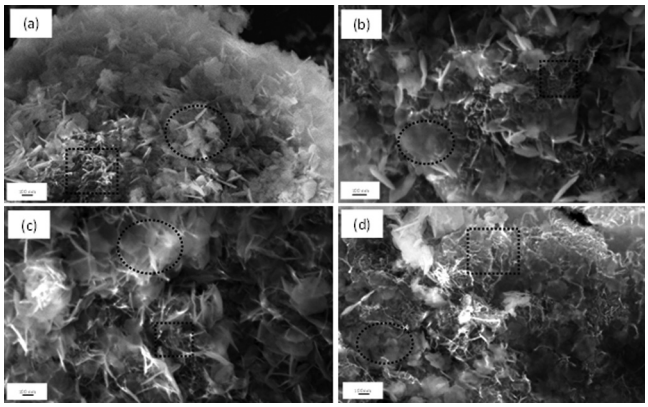

Fig. 4. SEM images of: (a) MWNT/LDH_{hl}-20, (b) MWNT/LDH_{hl}-33, (c) MWNT/LDH_{hl}-50, and (d) MWNT/LDH_{hl}-67. For clarification: the area enclosed by the squares represents MWNT and by circles LDH.

may be open to debate, but it shares the characteristic that the catalyst particles are partly in contact with a second phase and partly exposed to the reactive medium. In situ EDS analysis performed on the as-synthesized and supported LDH/MWNTs samples confirmed the presence of C, O, Mg and Al, with an average Mg/Al ratio of 1.9 ± 0.05, close to the intended value [30]. TEM analysis allows a more detailed investigation of the local microstructure of these materials (specifically, the dispersion rather than distribution quality); the dimensions of the LDH hexagonal platelets (Fig. 5) can also be determined although they are quite varied. For the hydrated samples, the average lateral size was found to be comparable for all the hybrid MWNT/LDH_{hl} samples, at approximately 62 ± 2 nm (see Supplementary data). This value is not comparable with those calculated from the Scherrer equation (~20 nm); the difference is attributed to bending of larger sheets. Pure LDH_{hl} showed a slightly bigger average lateral size (69 ± 2 nm), in agreement with the XRD trends. On average, larger LDH platelets were observed after hydration than for the as-synthesized MWNT/LDH (30 nm) [30]; a similar trend was observed for CNF/LDH hybrids [28]. The most significant result, that the LDH platelets become thinner in the MWNT hybrids, is more accurately observed by XRD.

The BET surface areas of all samples decreased slightly after the hydration process (Fig. 6), which is consistent with the increase in LDH platelet size, indicated by the XRD and TEM shape analysis. Generally, the BET surface area of the MWNT/LDH_{hl} catalysts increases with the MWNT content, as found previously for the

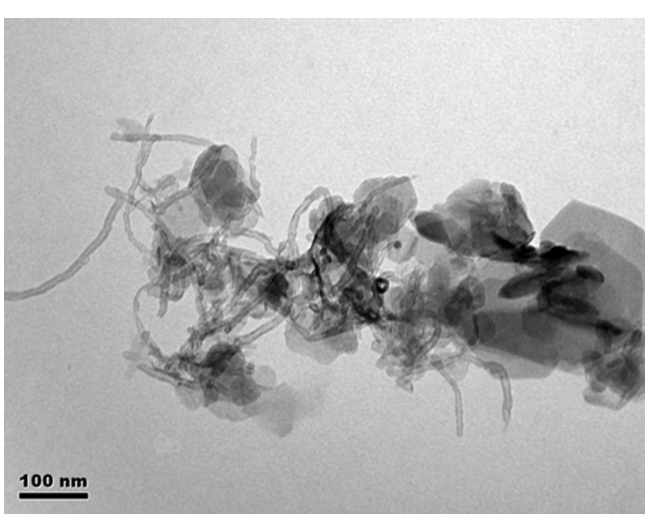

Fig. 5. TEM image of MWNT/LDH_{hl}-50 catalyst.

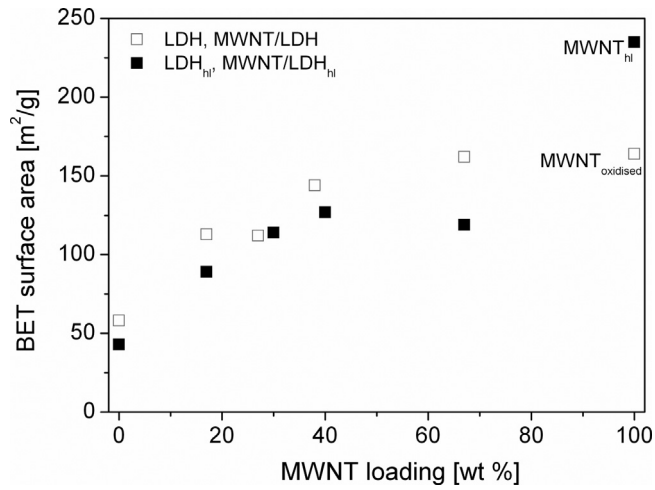

Fig. 6. BET surface areas of LDH, LDH_{hl}, $MWNT_{oxidized}$, $MWNT_{hl}$, MWNT/LDH, and MWNT/LDH_{hl} vs. MWNT loading (wt%).

as-synthesized hybrid samples [30]. BET surface areas of simple mixtures between LDH_{hl} and $MWNT_{hl}$ should follow a linear correlation traced between both pure materials. However, the BET values for the MWNT/LDH_{hl} catalysts instead follow a slight super-linear curvature (with the exception of the MWNT/LDH_{hl}-67 sample; Fig. 6). This trend is consistent with the changes in intrinsic crystal morphology, identified by XRD and TEM analysis, specifically the reduced LDH platelet thickness in the presence of MWNTs. However, there may also be a variation in the MWNT or LDH packing efficiency, which may in turn impact upon the final BET values determined for the hybrids catalysts; MWNT packing is known to be affected by degree of oxidation and capillarity effects [35]. The MWNT/LDH_{hl}-67 sample does not follow the BET curve; this difference may be attributed to the phase segregation that was observed for this catalyst in SEM, combined with the relatively weak size effects observed in XRD.

In general, all the samples show a hysteresis loop typical of mesoporous materials (type IV isotherm according to the IUPAC classification – see Supplementary data). The Barrett–Joyner–Halenda (BJH) model pore distribution confirms the mesoporosity of both supported and unsupported materials. The sharp peak between 2 and 4 nm is an artifact of the BJH model due to closing of the hysteresis loop [36].

The strength of basic centers is often evaluated from the maximum temperature at which the CO_2 desorption peak appears: the higher the temperature the stronger the basic sites. The strength and distribution of the basic sites found on the unsupported LDHs were determined from the TPD profiles of adsorbed CO_2 (Fig. 7). The $LDH_{as\text{-}synthesized}$ sample, as a reference, shows a peak centered around 673 K, generated by the decomposition of the carbonates inherently incorporated within the structure. In contrast, after activation, the CO_2 desorption peak for LDH_{hl} appears at higher temperatures (~750 K), consistent with the formation of basic sites, as expected. It is worth noting here that the hydroxyl groups of the hydrated LDH (basic sites of medium strength) are the active centers for the self-condensation of acetone [10,19], and that Abello et al. [6] associated the CO_2 desorption peak around 700–750 K with these sites. In this study, the peak centered at ~750 K, is observed for all four supported MWNT/LDH_{hl} catalysts but not for the as-synthesized LDH. This peak is consistent with the presence of such active centers in the rehydrated samples, which are necessary for effective catalysis (Fig. 8). A control TPD-CO_2 experiment on the $MWNT_{hl}$ identified a small amount of CO_2 desorption, which can be attributed both to the presence of physisorbed CO_2 and, more significantly, to the decomposition of surface oxide

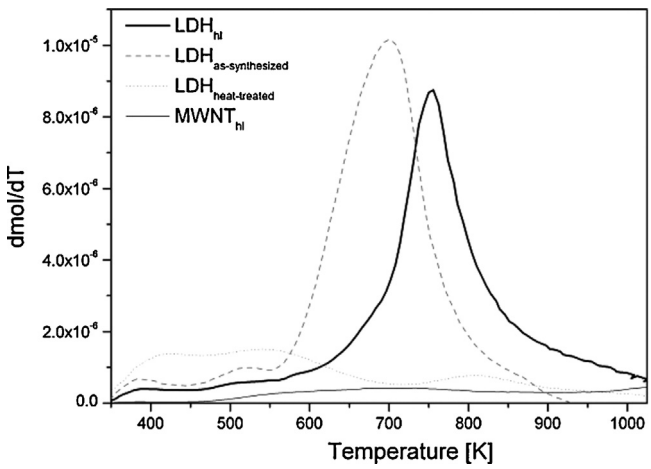

Fig. 7. CO_2 evolved during temperature-programmed desorption experiments over unsupported samples: LDH_{hl}, $LDH_{as-synthesized}$, $LDH_{heat-treated}$ and $MWNT_{hl}$.

groups, particularly carboxylic acids. However, the total amount of desorbed CO_2 is relatively low compared to all the LDH-containing samples (<10%), and so the fractional $MWNT_{hl}$ contribution to the MWNT/LDH_{hl}TPD-CO_2 profiles can be neglected. For the LDH_{hl} catalyst and all four MWNT/LDH_{hl} catalysts, the total amount of desorbed CO_2/g_{cat} and CO_2/g_{LDH} was determined (Table 1). Generally, within error, all the samples have a similar evolution of CO_2 as normalized to LDH content, though with slightly higher values for the supported catalysts.

3.2. Catalytic activity

The self-condensation of acetone was carried out over LDH_{hl}, $MWNT_{hl}$, and all the MWNT/LDH_{hl} composites. Selectivity to DAA was 100% for all the samples with the exception of $MWNT_{hl}$, which was found to be inactive, as expected. The final conversion (see Supplementary data) followed the initial rates, consistent with a deactivation of the catalyst over the long timescale of the reaction, possibly due to contamination of the surface by heavier products from continued condensations or adventitious atmosphere. It should be noted that the reaction was carried out at 273 K in order to achieve complete selectivity to DAA, suppressing the formation of mesityl oxide, which is normally produced from the dehydration of DAA [37]. In order to compare the catalyst performance, initial

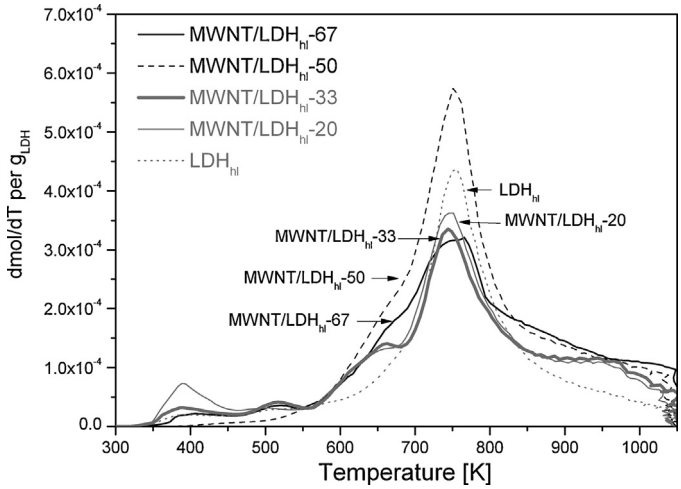

Fig. 8. CO_2 evolved per unit mass of active material during TPD experiments over LDH_{hl} and MWNT/LHD_{hl} samples.

rates of production of diacetone alcohol (DAA) were calculated. The initial rate values are calculated as the amount of DAA produced per hour and per unit mass of LDH with the error estimated by polynomial fitting. As shown in Table 1, initial rates for the supported samples, normalized per gram of LDH, first increase when the LDH is dispersed onto the MWNTs, but then surprisingly decrease as the MWNT content is increased further. The activity normalized per gram total catalyst shows the same trend, but even more strongly since the $MWNT_{hl}$ does not directly contribute to the reaction. Significantly, the activity of MWNT/LDH_{hl}-20 is remarkably high, almost 3-times higher than the pure LDH_{hl} catalyst (per gram LDH). Similarly, MWNT/LDH_{hl}-33 and MWNT/LDH_{hl}-50 show initial rates around 2-times greater than LDH_{hl}. These results demonstrate that utilizing $MWNT_{hl}$ as a support has a positive effect on the catalytic properties of the LDH_{hl}. Previous work on CNF/LDH systems [24,25] tabulated a 4-fold increase in activity per gram of LDH using a more diluted content of LDH onto the support than in the present work (11% vs. 80% LDH, respectively). However, the more diluted samples in the current study show a dramatic decrease rather than further increase in activity, suggesting an inhibiting effect associated with the MWNT component. One hypothesis is that carboxylated polyaromatic hydrocarbons, generated during the initial MWNT oxidation process (known as 'oxidation debris' or 'carboxylated carbonaceous fragments' [38]) may block the active sites. Although thoroughly washed with dilute base, according to previous protocols, additional debris may be released from the oxidized MWNTs under the more aggressive LDH synthesis conditions using concentrated base at elevated temperature.

In order to test this theory, a control sample was produced by treating the standard dilute-base washed oxidized MWNTs with a high pH solution mimicking the LDH synthesis liquor; solubilization of additional oxidation debris was observed, and the material added to LDH to test the effect on catalytic activity. After activation, the self-condensation of acetone was carried out in the presence of this carbonaceous debris LDH reference sample; the initial rate of reaction was very slow, at least one order of magnitude slower than all the other catalysts with the exception of the MWNT/LDH_{hl}-67 sample. It is reasonable that the carboxylated fragments may bind to the basic sites in the LDH, but not be cleanly removed, during activation. It is also possible that some of the wide range of oxygen-containing groups on the debris may participate in the condensation reaction, producing larger insoluble networks. At longer times over 100 h, deactivation of the catalyst was observed. Due to the debris, a high dilution of LDH on larger proportion of MWNTs is not useful with the current protocol. However, in any case, large dilutions of the active material are not practically attractive due to the large mass/volume of the gross catalyst system. The MWNT/LDH-20 systems offer an encouraging improvement in absolute activity per gram of supported catalyst (LDH + MWNT), compared to the CNF system in the literature (162 vs. 61 $mmol_{DAA}\ g_{cat}^{-1}\ h^{-1}$, respectively) [24].

Structure–activity correlations with respect to unsupported activated LDHs have been widely discussed in the literature. The Brønsted-base sites (OH^-) associated with the hydration of the LDH interlayer are reported to be the active centers over which the self-condensation of acetone to DAA occurs [10,19]. However, alternative suggestions have been given as to the nature and accessibility of these active basic sites. Previously, the activity was correlated to the total BET surface area of activated LDH materials; however, more recently it was reported that after activation, the active basic centers are exclusively situated at the edges of the LDH platelets instead of across the total surface area [6,16,20,24,39]. Consequently, several studies have been carried out with the aim of increasing the number of active sites on the edges of the platelets sites by decreasing the lateral LDH particle size [6,13,17,18,20,24,28]. In particular, Winter et al. [24] and

Alvarez et al. [28] achieved a reduced LDH platelet size (~20 nm compared to the commonly reported ~60 nm) by supporting LDH materials on carbon nanofibers (CNFs). Improved catalytic activity of these catalysts was partially attributed to the reduction of the LDH platelet size, and additionally, it was suggested that accessibility to the active centers was enhanced due to the pore system of the CNFs. In the current study, slightly smaller LDH particles (lateral size) and thinner crystallites were observed when supporting the LDH on MWNT compared with pure LDH_{hl} (Fig. 3). Decreased LDH crystallite sizes (i.e. higher BET surface area of the active material) may partly explain the improved catalytic properties of the MWNT/LDH_{hl} catalysts compared to the unsupported material. Amongst the MWNT/LDH_{hl} hybrids, the LDH crystallite thicknesses very slightly decrease with increasing the weight percentage of MWNT (Fig. 3). However, the catalytic activity does not follow the same trend; in fact, the most active catalyst (MWNT/LDH_{hl}-20) contains the lowest MWNT loading. Therefore, whilst the presence of some MWNTs are beneficial for catalytic activity, helping to nucleate more active LDH particles as well as potentially improving accessibility, the associated debris studied previously also inhibits the reaction at high MWNT loadings. There is a correlation of the initial rate of DAA formation per unit mass of LDH with concentration of the specific basic sites (i.e. active centers), as assigned to the desorption peak at ~750 K by TPD-CO_2 (Table 1). The number of active centers may be related to the LDH particle size, or rather to the surface area accessible to acetone, but also to the number of defects in the LDH structure, which might also act as active basic centers as suggested by Chimentao et al. [26]. Additionally, the uniform dispersion of the LDH particles on the porous MWNT network, as indicated from the electron microscopy analyses for all the active hybrids, should improve access to the active basic centers, increasing the catalytic performance of the catalysts. However, it should be noted that the initial rates are not directly proportional to the number of active centers accessible to CO_2, which might imply either that not all active centers are accessible to the acetone during reaction [22] or that they are not equally active. Indeed the [$mmol_{acetone}\ mm_{total\ desorbed\ CO2}{}^{-1}\ h^{-1}$] values shown in Table 1, show that the catalytic centers are more active for the majority of the MWNT supported samples, but with a systematic decrease in increasing MWNT content. This result is consistent with a direct enhancement of the intrinsic activity of the LDH, due to the presence of MWNTs as a support and nucleating agent, but an inhibition due to increasing debris content.

4. Conclusion

Depositing LDH onto oxidized commercially-available MWNTs supports leads to an improved catalytic performance in the self-condensation of acetone relative to the pure LDH catalyst. Smaller LDH crystallite sizes and a good dispersion of the LDH particles on the MWNTs increase the number of active centers accessible to acetone, and their activity. The active basic centers of MWNT/LDH_{hl} catalysts, quantified by CO_2-TPD, correlate qualitatively with the catalytic activity, though the [$mmol_{acetone}\ mm_{total\ desorbed\ CO2}{}^{-1}\ h^{-1}$] results indicate varying effectiveness. At the same time, it seems that the presence of the oxidized MWNTs is detrimental, hindering the reaction by contaminating the active sites during synthesis, activation, or the catalytic reaction itself. Specifically, contamination of the LDH material, during its synthesis, by polycarboxylated debris from the CNT oxidation reaction, is the likely reason for the deactivation. The washing treatment applied to the oxidized nanocarbon before catalyst deposition should, therefore, be designed to mimic subsequent synthesis conditions, to ensure that all mobile contaminants are removed. It is also interesting to note that the character of the oxidation debris is similar to graphene oxide materials that might be considered as potential support materials [40].

There is an optimum concentration of MWNTs that balances the benefits of the support against its additional mass/volume as well as the inhibition effect. In this study, the optimum MWNT-content was found to be 20%, (MWNT/LDH_{hl}-20), offering 3-times higher specific activity than the pure LDH_{hl} catalyst, and an improvement in activity per gram of supported catalyst compared to studies of CNFs. However, further optimization of these catalysts should be carried out to determine the maximum activity that can be achieved using MWNT/LDH_{hl} composite materials, if the adverse effects of MWNTs/contaminants are kept to a minimum. Investigation of alternative MWNT functionalization processes, which stabilize the LDH deposition without introducing contaminating debris or other chemically-active groups might be the key to improving further the catalytic performance of MWNT/LDH_{hl} catalysts [41]. These solid base MWNT/LDH catalysts may also be useful in other reactions for example the gas-phase self-condensation of acetone [42] or other liquid-phase condensation reactions (aldol, Knoevenagel and Claisen-Schmidt condensation reactions), as well as Michael additions, phenol alkylations or epoxidation of olefins [5,12,16,43]. Previous studies showed an improved stability of the LDH when supported on MWNTs during cyclic gas phase adsorption processes. These data suggest that the hybrids may be stable to regeneration and reuse, following straightforward recovery through filtration or sedimentation, making them interesting for industrial application.

Acknowledgments

The authors are grateful to David Chadwick, Felicity Sartain, Ainara Garcia-Gallastegui, Maurice C.D. Mourad and Neal Skipper for discussions and help during experiments. Financial support for this project was provided by the Deanship of Scientific Research at King Abdulaziz University D/05/432 and scholarships from CONACyT and SEP.

Appendix A. Supplementary data

Supplementary data associated with this article can be found, in the online version, at http://dx.doi.org/10.1016/j.molcata.2014.11.002.

References

[1] G.S. Salvapati, K.V. Ramanamurty, M. Janardanarao, J. Mol. Catal. 54 (1989) 9–30.
[2] P.D.S.A.J. Papa Jr., Kirk-Othmer Encyclopaedia of Chemical Technology, Wiley, Toronto, Canada, 1978.
[3] J.A.M.A. Cybulski, M.M. Sharma, R.A. Sheldon, Fine Chemicals Manufacture: Technology and Engineering, 2001.
[4] K. Tanabe, W.F. Hölderich, Appl. Catal. A: Gen. 181 (1999) 399–434.
[5] F. Figueras, Top. Catal. 29 (2004) 189–196.
[6] S. Abelló, F. Medina, D. Tichit, J. Pérez-Ramírez, J.C. Groen, J.E. Sueiras, P. Salagre, Y. Cesteros, Chem. – A Eur. J. 11 (2005) 728–739.
[7] M. Lakshmi Kantam, B.M. Choudary, C. Venkat Reddy, K. Koteswara Rao, F. Figueras, Chem. Commun. (1998) 1033–1034.
[8] J.C.A.A. Roelofs, A.J. van Dillen, K.P. de Jong, Catal. Lett. 74 (2001) 91–94.
[9] D. Tichit, C. Gérardin, R. Durand, B. Coq, Top. Catal. 39 (2006) 89–96.
[10] D. Tichit, M. Naciri Bennani, F. Figueras, R. Tessier, J. Kervennal, Appl. Clay Sci. 13 (1998) 401–415.
[11] F. Winter, A. Jos van Dillen, K.P. de Jong, J. Mol. Catal. A: Chem. 219 (2004) 273–281.
[12] F. Cavani, F. Trifirò, A. Vaccari, Catal. Today 11 (1991) 173–301.
[13] M.a.J. Climent, A. Corma, S. Iborra, A. Velty, J. Mol. Catal. A: Chem. 182–183 (2002) 327–342.
[14] M.J. Climent, A. Corma, S. Iborra, A. Velty, Catal. Lett. 79 (2002) 157–163.
[15] M.J. Climent, A. Corma, S. Iborra, A. Velty, Green Chem. 4 (2002) 474–480.
[16] J.C.A.A. Roelofs, A.J. van Dillen, K.P. de Jong, Catal. Today 60 (2000) 297–303.
[17] W.T. Reichle, J. Catal. 94 (1985) 547–557.
[18] S. Abello, F. Medina, D. Tichit, J. Perez-Ramirez, Y. Cesteros, P. Salagre, J.E. Sueiras, Chem. Commun. (2005) 1453–1455.

[19] K.K. Rao, M. Gravelle, J.S. Valente, F. Figueras, J. Catal. 173 (1998) 115–121.
[20] J.C.A.A. Roelofs, D.J. Lensveld, A.J. van Dillen, K.P. de Jong, J. Catal. 203 (2001) 184–191.
[21] D. Tichit, B. Coq, S. Cerneaux, R. Durand, Catal. Today 75 (2002) 197–202.
[22] F. Winter, X. Xia, B.P.C. Hereijgers, J.H. Bitter, A.J. van Dillen, M. Muhler, K.P. de Jong, J. Physi. Chem. B 110 (2006) 9211–9218.
[23] M. Mokhtar, A. Inayat, J. Ofili, W. Schwieger, Appl. Clay Sci. 50 (2010) 176–181.
[24] F. Winter, V. Koot, A.J. van Dillen, J.W. Geus, K.P. de Jong, J. Catal. 236 (2005) 91–100.
[25] F. Winter, A.J. van Dillen, K.P. de Jong, Chem. Commun. (2005) 3977–3979.
[26] R.J. Chimentão, S. Abelló, F. Medina, J. Llorca, J.E. Sueiras, Y. Cesteros, P. Salagre, J. Catal. 252 (2007) 249–257.
[27] F. Winter, Hydrotalcite-based Catalysts for the Synthesis of Methyl Isobutyl Ketone, University Utrecht, 2006.
[28] M.G. Álvarez, A.M. Frey, J.H. Bitter, A.M. Segarra, K.P. de Jong, F. Medina, Appl. Catal. B: Environ. 134–135 (2013) 231–237.
[29] E. Auer, A. Freund, J. Pietsch, T. Tacke, Appl. Catal. A: Gen. 173 (1998) 259–271.
[30] A. Garcia-Gallastegui, D. Iruretagoyena, M. Mokhtar, A.M. Asiri, S.N. Basahel, S.A. Al-Thabaiti, A.O. Alyoubi, D. Chadwick, M.S.P. Shaffer, J. Mater. Chem. 22 (2012) 13932–13940.
[31] J. Cho, A.R. Boccaccini, M.S.P. Shaffer, Carbon 50 (2012) 3967–3976.
[32] R. Verdejo, S. Lamoriniere, B. Cottam, A. Bismarck, M. Shaffer, Chem. Commun. (2007) 513–515.
[33] J.I. Langford, A.J.C. Wilson, J. Appl. Crystallogr. 11 (1978) 102–113.
[34] D. Tichit, M.N. Bennani, F. Figueras, J.R. Ruiz, Langmuir 14 (1998) 2086–2091.
[35] M.S.P. Shaffer, X. Fan, A.H. Windle, Carbon 36 (1998) 1603–1612.
[36] J.C. Groen, L.A.A. Peffer, J. Pérez-Ramírez, Microporous Mesoporous Mater. 60 (2003) 1–17.
[37] G.G. Podrebarac, F.T.T. Ng, G.L. Rempel, Chem. Eng. Sci. 52 (1997) 2991–3002.
[38] C.G. Salzmann, S.A. Llewellyn, G. Tobias, M.A.H. Ward, Y. Huh, M.L.H. Green, Adv. Mater. 19 (2007) 883–887.
[39] B.F.S.M.B.J. Roeffaers, H. Uji-i, F.C. De Schryver, P.A. Jacobs, D.E. De Vos, J. Hofkens, Nature 439 (2006) 572–575.
[40] A. Garcia-Gallastegui, D. Iruretagoyena, V. Gouvea, M. Mokhtar, A.M. Asiri, S.N. Basahel, S.A. Al-Thabaiti, A.O. Alyoubi, D. Chadwick, M.S.P. Shaffer, Chem. Mater. 24 (2012) 4531–4539.
[41] R. Menzel, M.Q. Tran, A. Menner, C.W.M. Kay, A. Bismarck, M.S.P. Shaffer, Chem. Sci. 1 (2010) 603–608.
[42] S. Ordóñez, E. Díaz, M. León, L. Faba, Catal. Today 167 (2011) 71–76.
[43] M.J. Climent, A. Corma, S. Iborra, K. Epping, A. Velty, J. Catal. 225 (2004) 316–326.